Distribution Agreement

In presenting this thesis as a partial fulfillment of the requirements for a degree from Emory University, I hereby grant to Emory University and its agents the non-exclusive license to archive, make accessible, and display my thesis in whole or in part in all forms of media, now or hereafter now, including display on the World Wide Web. I understand that I may select some access restrictions as part of the online submission of this thesis. I retain all ownership rights to the copyright of the thesis. I also retain the right to use in future works (such as articles or books) all or part of this thesis.

Jake McGrath April 3, 2021

Hydrophobicity's Role in Electrostatic Charge Decay of Levitated Solids

by

Jake McGrath

Justin C Burton
Adviser

Department of Physics

Justin C Burton

Adviser

Effrosyni Seitaridou

Committee Member

Paul Oser

Committee Member

2021

Hydrophobicity's Role in Electrostatic Charge Decay of Levitated Solids

By

Jake McGrath

Justin C Burton

Adviser

An abstract of
a thesis submitted to the Faculty of Emory College of Arts and Sciences
of Emory University in partial fulfillment
of the requirements of the degree of
Bachelor of Science with Honors

Department of Physics

2021

Abstract

Hydrophobicity's Role in Electrostatic Charge Decay of Levitated Solids

By Jake McGrath

Electrically charged particles suspended in gas exist in numerous planetary environments. Salient examples include volcanic plumes, airborne Saharan sand, Martian dust devils, and the dune fields of Titan. Yet the microphysical processes that lead to electrification are not well understood. Moreover, the lifetime of charge on electrified particles is not well quantified and the events preceding electrostatic neutrality are poorly understood. Our laboratory measurements aim to answer these questions through acoustic levitation to ensure that charge is not lost through physical contact or through any other mechanism of charge transfer other than the natural processes of charge loss. Two hemispherical transducers produce an acoustic standing wave that lofts particles of millimetric scale. An ionizer then charges these particles, and the remaining charge is measured over days or weeks by moving the particle through a Faraday cup.

Previous measurements showed that the lifetime of charge is dependent on the relative humidity of its environment. These measurements, however, were limited to low-density, porous particles. Now we have constructed an acoustic levitation device capable of suspending dense materials such as copper. Additionally, in environments of varying humidity, we investigate the mechanisms leading to airborne particle charge loss, and its relation to the material's hydrophobicity. We find that water dissociation is the dominate mechanism of charge transfer in these systems.

Hydrophobicity's Role in Electrostatic Charge Decay of Levitated Solids

By

Jake McGrath

Justin C Burton

Adviser

A thesis submitted to the Faculty of Emory College of Arts and Sciences
of Emory University in partial fulfillment
of the requirements of the degree of
Bachelor of Science with Honors

Department of Physics

2021

Acknowledgements

I would like to thank former Burton Lab members Tianshu Huang (Graduate Student, Department of Applied Physics, Yale University) and Brady Wu (Graduate Student, Department of Physics, University of Chicago) for helping me become accustomed to academic research. I would like to acknowledge Dr. Joshua Méndez-Harper for recruiting me to Burton Lab, and for his continued support, advice, and direction on our current projects in the lab. I appreciate the time that each of my committee members have allotted to help oversee this project, and I express great gratitude to Dr. Seitaridou who inspired me to become a physicist. Lastly, I would like to thank Dr. Burton for his continued support and motivation. Your personal and academic advice encouraged me to enroll in graduate school, and hopefully earn a doctorate degree one day.

Table of Contents

List of Tables and Figures

Chapter 1

Introduction

1.1 Motivations from Nature

Charging of granular systems occur in a wide variety of natural events. When dusty systems experience a disturbance, friction and random particle collisions lead to charge transfer. Charged granular systems can accelerate natural processes and carry a wide variety of applications. In deep-space, electrostatic forces can accelerate the formation of planetesimals in protoplanetary disks [1]. On Mars, dust devils accumulate massive amounts of charge which can alter the global chemical composition of the red planet. Electrostatic charge created during dust devils can break apart carbon dioxide and water molecules to form hydrogen peroxide and ozone molecules [2] [32]. Furthermore, volcanic plumes on Earth can create a separation of charge great enough for discharge – also called volcanic lightning. Volcanic lightning acted as a natural chemical reactor before life on Earth by synthesizing and ejecting organic compounds at near supersonic speeds into the troposphere and stratosphere, where further photochemical processing occurred [3].

During the Harmattan season in North and West Africa, northeasterly trade winds sweep across the Sahara Desert lifting dust and sand from the desert floor. The dust travels 3,000 miles across the Atlantic Ocean to the Amazon rainforest. Launched in 2006, NASA's CALIPSO satellite has been studying the transport properties of these granular plumes as they travel westward. CALIPSO finds that an average of 182 million tons of dust leaves Africa each year, but only around 27 million tons reach the Amazon [4]. The dust leaving Africa contains plentiful

nutrients necessary for life. Phosphorus, for example, constitutes 0.08% of the dust leaving the Sahara [5]. As the constant rainfall of the Amazon washes away critical nutrients, the Amazon can be phosphorous deficient by up to 90 percent. The 22 thousand tons of phosphorous transported from the Sahara are required for replacing lost nutrients and for supporting the global biome [6].

When granular systems become airborne, random collisions and interactions cause particles to exchange charge. Typically, larger particles retain positive charge and smaller particles charge negatively. In Saharan dust storms, triboelectric charging can create electric fields of intensities in excess of 11 kilovolts per meter [7]. An electric field of that magnitude is comparable to field strengths measured less than a kilometer away from the edge of a thunderstorm [8]. It is well known that the electrification of granular particles and intense electric fields play a critical role in the lifting and transport of dusty systems [9] [10]. A system of light-weight charged particles could easily experience deviations from its original trajectory due to electrostatic forces. Moreover, these forces can lift charged particles, while neutral grains are less likely to be airborne. The period of a grain's levitation is dependent on the magnitude of its charge, and how long it can retain this charge. This phenomenon of electrically charged airborne materials is widely observed in nature, however, neither the lifetime nor the stability of charge in lofted granular systems are well quantified.

1.2 Lifetime of Charge

Although we observe airborne charged particles in nature and understand the importance of these systems, the stability of charge and the timescales of a particle's inevitable electrostatic

neutrality are not well quantified. One reason for our lack of understanding is that reaching airborne electrically charged dusty systems in nature is challenging. Conducting experiments inside of a dust storm, for example, are dangerous and expensive. Moreover, many laboratory experimental methods of charge measurement require physical contact with the charged object. This measurement method may read an inaccurate lifetime of charge on the particle. In experiments without acoustic levitation, the charged object has a path to electrical ground, and shorter than expected charge life measurements are observed. Our implementation of acoustic levitation as a novel scientific tool erases these sources of error. From the moment that we begin an experiment to sometime later when the particle has no residual charge left, the experimenter does not come into contact with the particle. Although acoustic levitation requires contact with air – which is what we find with electrically charged particles in nature – the particle does not come to contact with any external path to electrical ground. Therefore, the charge must be transferred entirely through the surrounding air. The timescales that we measure through our charge sensing acoustic levitator reflect the timescales of charge leakage in nature.

In 1995, Tada and Murata studied the timescales of electrostatic charge loss on a 19mm steel sphere [11]. In their experiment, the steel was suspended by a Teflon cable. Teflon – a component often used in electrical tape – is resistive to charge transfer due to high bulk resistivity. Therefore, the paper was able to infer that any net loss of charge must have been lost through the surrounding air. Tada and Murata were able to show in Figure 1.1 that charge is lost at characteristically faster rates in humid environments relative to dry environments.

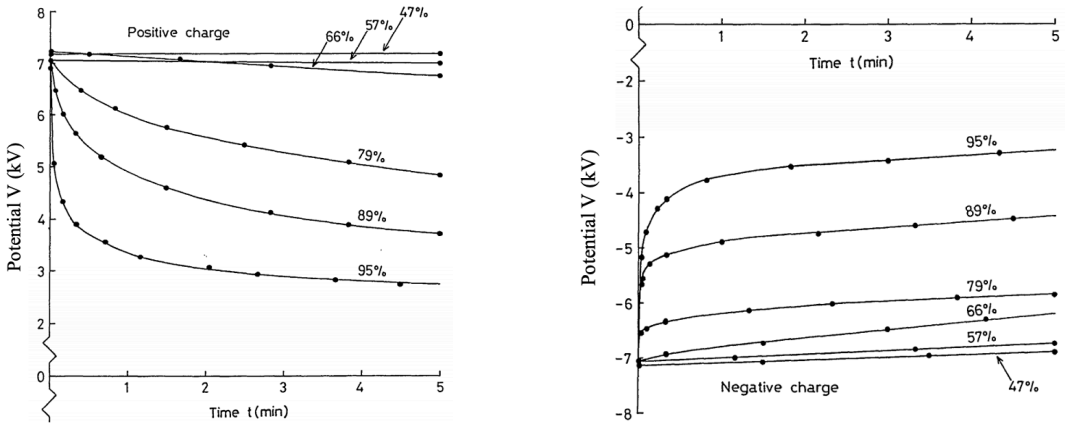

Figure 1.1: Rate of charge leakage in various humid environments. Figure from Tada and Murata's paper [11]. Charge is lost faster in humid environments. The lifetime of charge is described in minutes, maybe an hour or so in dry environments.

Although they were able to qualitatively show that the rate of charge loss is a function of humidity, a more detailed analysis is needed. Moreover, more knowledge is needed on the microphysical processes that lead to electrostatic neutrality, and how these mechanisms of charge transfer relate to the material's hydrophobicity.

Preliminary results from the Burton Lab at Emory University have not drawn similar conclusions as Tada and Murata did. Tada and Murata found that charge existed on the steel sphere for a few minutes whereas our acoustic levitation design found that particles suspended in dry environments (relative humidity < 50%) retained residual charge for days, or even up to a week. On the other hand, when immersed in humid environments (relative humidity > 50%), the particle would lose all of its electrostatic charge in a day, or even in a matter of a couple hours. The assumption that charge was not lost through the Teflon cable was incorrect. Our acoustic levitator has shown that two different mechanisms of charge transfer appear to be dominating the rate of charge loss in dry and wet environments.

Our preliminary results only tested very low density, small polystyrene spheres (diameter < 1mm and $\rho = 0.05 \frac{g}{cm^3}$) due to limitations of the original acoustic levitation device. Porous materials with extremely low densities are not indicative of the triboelectrically charged lofted materials that we observe in nature. Moreover, polystyrene is known to be hydrophobic with a water contact angle of 90°. Considering how the humidity of the environment plays a crucial role in the characteristic timescale of charge decay, we hypothesize that the wettability of the particle itself may affect the observed timescale. Naturally, hydrophilic particles will accumulate water films and should lose charge faster. Hydrophobic particles, however, will not accumulate thick films of water and should retain charge for longer periods of time. With unanswered questions and possible sources of error, it was necessary to improve our understanding of how water layers form in humid environments. We also needed to improve our acoustic levitation capabilities if we wished to study charge decay from an array of levitated materials.

Between these preliminary Burton Lab measurements and the results of Tada and Murata's paper, we understand well that the rate of charge leakage is proportional to the humidity of the environment. Now, the question is whether the microphysical processes involved that lead to electrostatic neutrality depend on the material's hydrophobicity. In order to test this hypothesis, we constructed a new acoustic levitation device. The new levitator supplies an acoustic radiation force of over 180 times greater than before. Whereas before we were limited to levitating polystyrene, now we can levitate copper, steel, and brass on the upper end. Most importantly, however, we are now able to levitate glass. Glass is unique because it can be coated with a variety of hydrophobic and hydrophilic films. Therefore, we can coat an array of glass particles in varying

hydrophobic and hydrophilic films and test if the characteristic timescale of charge leakage is a function of both humidity and material hydrophobicity.

To supplement this data, a Quartz Crystal Microbalance (QCM) is implemented to understand the rate of water film formation in humid environments. A QCM is a piezoelectric vibrator that oscillates at a resonate frequency. When water vapor condenses on the surface of the QCM, the increased mass slows the rate of oscillation. From the frequency shift, a film thickness is calculated. We expect to find that a QCM with hydrophobic properties should not be suscept to thick water films, and the corresponding hydrophobic glass-coated particle should retain its charge for a long period. Conversely, a hydrophilic QCM surface should flood with water layers and the corresponding hydrophilic glass-coated particle should lose its electrostatic charge relatively quickly.

In this essay, the processes of constructing the new acoustic levitation device, the design of the new electrostatic charge measurement system, and the mechanisms of charge transfer in high and low humidities will be explored. The supplementing hydrophobicity-QCM measurements and how this relates to the characteristic charge decay times are presented. Finally, a bridge between the lifetime of charge on levitated solids and surface wettability is created.

Chapter 2

Acoustic Levitation as a Novel Scientific Tool

2.1 Acoustic Levitation Background

2.1.1 Sound and the Acoustic Radiation Force

Sound is a longitudinal pressure wave that propagates through some medium. As a sound wave travels through air, molecules are compressed into regions of high density and pulled apart in regions of low density. Because sound is a wave, some percentage of the wave will be reflected and some will be transmitted when it comes into contact with a new medium. Moreover, sound waves can interfere constructively and destructively. Acoustic levitation utilizes these interference properties of sound waves to create a standing wave [12] [13]. A standing wave (or a stationary wave), whose wavefunction is independent of time, is the results of wave superposition. When two sound waves of the same frequency are fired in opposite directions, regions of constructive and destructive interference are formed. In areas of destructive interference (called nodes), there is little wave movement, thus there is little pressure. Conversely, at areas of constructive interference (called antinodes), the pressure is maximized as the wave's resonance is maximized. Figure 2.1 examines a standing wave [14].

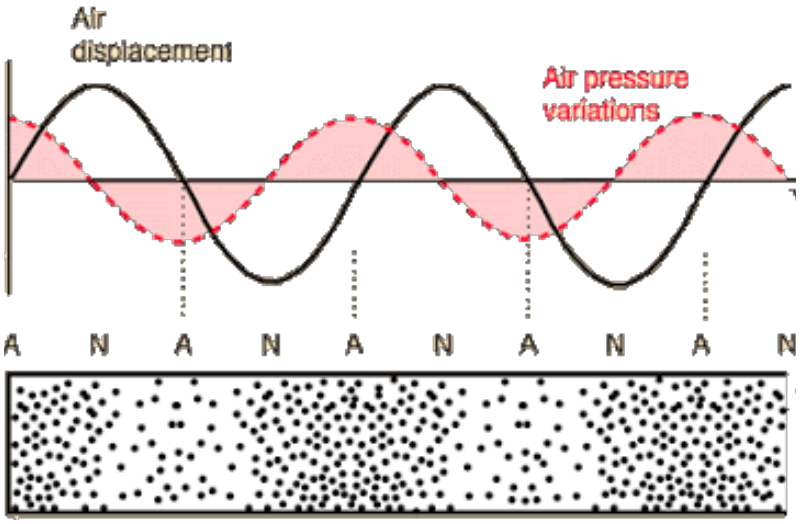

Figure 2.1: A standing wave in air. Image used from Georgia State University [14]. The antinodes correspond to regions of maximum pressure variations. The areas of destructive interference (where the red curve is zero) are called the nodes and have relatively lower pressure variation.

Acoustic levitation utilizes the power of high frequency sound waves and the properties of a standing wave to counteract the downward force of gravity. When a particle is placed within the standing wave of Figure 2.1, it will gravitate to the nearest node as it flows along the pressure gradient of the wave field. By simply balancing the forces exerted on the particle, if the particle's weight is less than the force supplied by the surrounding pressure field, the particle will levitate in air.

Russian-American physicist L.P. Gor'kov derived an expression for the acoustic radiation force on a spherical particle in 1961 [15] [16] [17]. The Gor'kov potential, given by Equation 2.1, describes the acoustic radiation potential surrounding a particle of radius R within the acoustic field.

$$U = \pi R^3 \left(\frac{\langle p^2 \rangle}{3\rho_0 c^2} f_1 - \frac{\rho_0 \langle u^2 \rangle}{2} f_2 \right) \tag{2.1}$$

$$f_1 = 1 - \frac{\rho_0 c^2}{\rho_s c_s^2}, \tag{2.2}$$

$$f_2 = 2\left(\frac{\rho_s - \rho_0}{2\rho_s + \rho_0}\right), \tag{2.3}$$

where $\langle p^2 \rangle$ and $\langle u^2 \rangle$ are the mean-squared values of the pressure and velocity fields of the wave. In Equations 2.1 - 2.3, the density of the medium and sphere are given by ρ_0 and ρ_s, and the speed of sound in the medium and in the levitated sphere are given by c^2 and c_s^2, respectively. Assuming that the levitated sphere is rigid, we have that $\rho_s \gg \rho_0$. Sound also travels faster through solid mediums, thus $c_s^2 \gg c^2$. Further analyzing Equations 2.2 and 2.3 for $\rho_s \gg \rho_0$ and $c_s^2 \gg c^2$, we can simply $f_1 \approx f_2 \approx 1$.

Moreover, the mean-squared values for the pressure and velocity fields are given by Equations 2.4 and 2.5 [18].

$$\langle p^2 \rangle = p_m^2 cos^2(kz), \tag{2.4}$$

$$\langle u^2 \rangle = \frac{p_m^2}{\rho_0^2 c^2} sin^2(kz), \tag{2.5}$$

where the k is the wave number $\frac{2\pi}{\lambda}$, and p_m denotes the maximum of the pressure field expressed as $2\pi\rho_0 c^2 \frac{d}{\lambda}$ for the wavelength λ and maximum air molecule displacement d. These terms are trigonometric functions in the direction along which the wave propagates (the vertical $\hat{z}$ direction).

The force of any potential field is given by Equation 2.6, allowing us to solve for the acoustic radiation force when the Gor'kov potential is substituted in.

$$F = -\nabla U \tag{2.6}$$

Substituting the mean-squared pressure and velocity fields into Equation 2.1, we can differentiate with respect to z in order to obtain our force equation. Assuming that the sphere is rigid such that $f_1 \approx f_2 \approx 1$, we arrive at Equation 2.7.

$$\overrightarrow{F_R} = \frac{5\pi}{6} \frac{p_m^2}{\rho_0 c^2} R^3 k \sin(2kz)\ \hat{z} \tag{2.7}$$

Where $\overrightarrow{F_R}$ denotes the acoustic radiation force in the vertical $\hat{z}$ direction. Note that the force is a sinusoidal function in the $\hat{z}$ direction. Therefore, as a test point travels vertically through the standing wave, it will reach points of minimum force (at the nodes where $\sin(2kz) = 0$) and points of maximum force (at the antinodes where $\sin(2kz) = 1$). Therefore, the maximum acoustic levitation force achieved at the antinode is given by Equation 2.8.

$$\left|\overrightarrow{F_R}\right|_{max} = \frac{5\pi}{6} \frac{p_m^2}{\rho_0 c^2} R^3 k = \frac{20\pi^4}{3} \rho_0 c^2 d^2 \left(\frac{R}{\lambda}\right)^3 \tag{2.8}$$

For levitation, the acoustic radiation force given by Equation 2.8 needs, at minimum, to match the weight of the levitated particle. Creating this inequality we arrive at Equation 2.9.

$$mg = \frac{4\pi}{3} R^3 \rho_s\, g \ \leq \ \frac{5\pi}{6} \frac{p_m^2}{\rho_0 c^2} R^3 k \tag{2.9}$$

Based on this expression, an engineer who wants to maximize the acoustic radiation force on some given particle of radius R will extract the adjustable parameters k and p_m. To construct an acoustic levitation device designed to maximize the lifting force, we want to maximize the amplitude of the pressure field for some large wave number k. The original acoustic levitation device used in preliminary Burton Lab experiments was limited in this sense. The adjustable parameters k and p_m were relatively weak, and we were limited to levitating small polystyrene beads. The construction of a new, stronger acoustic levitator was necessary in order to further study how charge decays from levitated solids of differing hydrophobicity.

2.1.2 The High-Powered Acoustic Levitation Device

The acoustic levitation device was constructed following the guidance of Marzo et al. [19]. The levitation device consists of two concave hemispheres lined with concentric circles of transducers. The transducers are controlled by an Arduino Uno device that feeds the system a sinusoidal signal. The Arduino is programmed to have the transducers operate typically between 30-40 kHz. With each hemisphere firing sound waves, the radiation force of this design is larger than other levitators with only one hemisphere and a reflector. As the sound waves from the two hemispheres propagate inwards, they interfere and create a standing wave. A particle placed within the wave field will move to a region of low pressure at the closest node, and it may levitate if the condition of Equation 2.9 is met. Figure 2.2 shows the acoustic levitation device constructed.

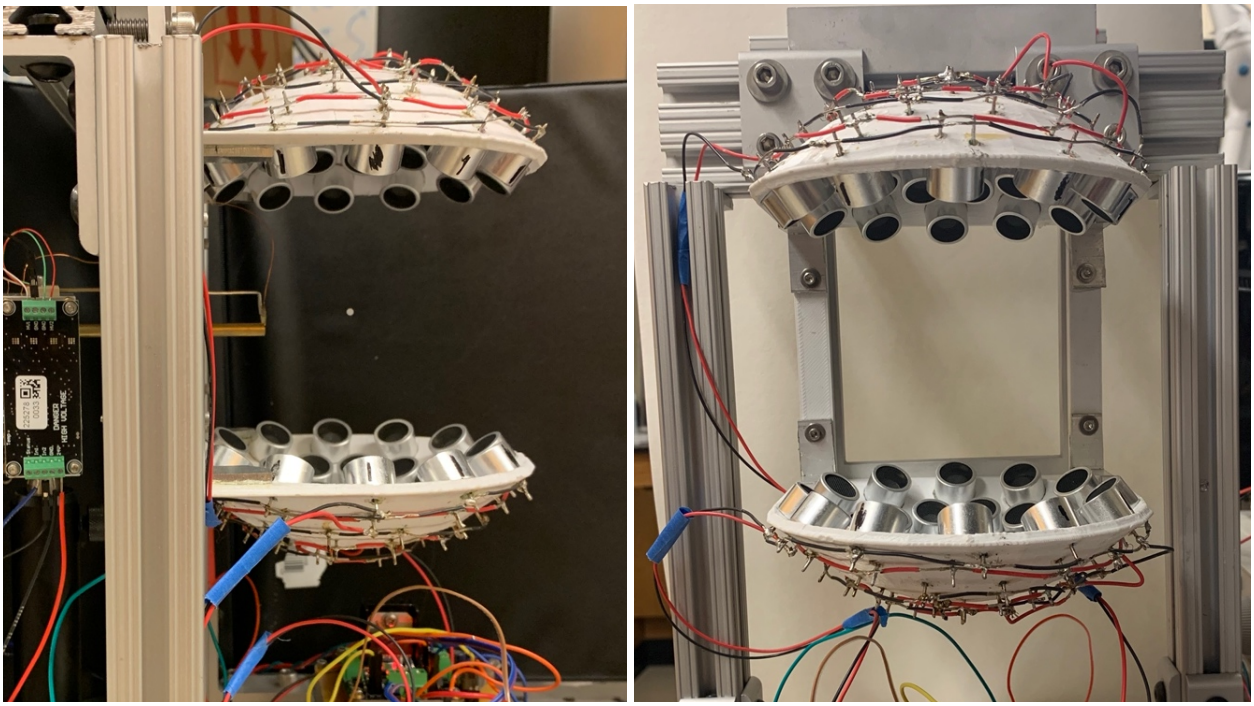

Figure 2.2: The charge sensing acoustic levitation device. Two hemispheres of transducers fire sound waves that interact and form a standing wave. If the acoustic radiation force supplied is larger than the particle's weight, it will levitate.

Acoustic levitation in our laboratory environment is constrained by two general limiting conditions. Firstly, frequencies of greater than 20 kHz are required to levitate macroscopic objects, or, more directly, the acoustic radiation force needs to exceed the particle's weight. Also, the diameter of the particle needs to be less than half of a wavelength. When the diameter is sufficiently small, the particle may rest in a node between two antinodes. Otherwise, the particle will begin to oscillate, become unstable, and fall out of the standing wave. Therefore, if we want to levitate larger objects of radius R, we need to increase the wavelength such that $2R \leq \frac{\lambda}{2}$. Examining Equation 2.8, we find that the magnitude of the acoustic radiation force is inversely proportional to the wavelength of the standing wave, λ, and positively correlated to the amplitude of the pressure field, p_m. Therefore, when increasing the wavelength to levitate larger particles, we effectively decrease the magnitude of the radiation force. With our old levitation device, this is where we were limited. To counteract the decreasing magnitude of the acoustic radiation force, we needed to increase the amplitude of the pressure field, however, we were unable to do so with weak transducers driving the standing wave. After constructing the levitator in Figure 2.2 with larger and more powerful transducers, the amplitude of the pressure field is sufficiently strong such that an increase in the wavelength has an insignificant effect on the magnitude of the acoustic radiation force. Thus, we are now able to levitate much larger particles.

In previous experiments, the levitation device was limited to polystyrene particles ($2R <$ 1 mm and $\rho = 0.05\ \frac{g}{cm^3}$). In a series of tests examining the limiting capabilities of the new acoustic levitator, we found that we could levitate an array of materials of varying volumes, densities, and hydrophobicities. Polystyrene, pumice, hydrogels, glass, and even some metals like

copper were within our levitation capabilities. Figure 2.3 shows suspended irregularly shaped pumice, two aluminum spheres, and copper.

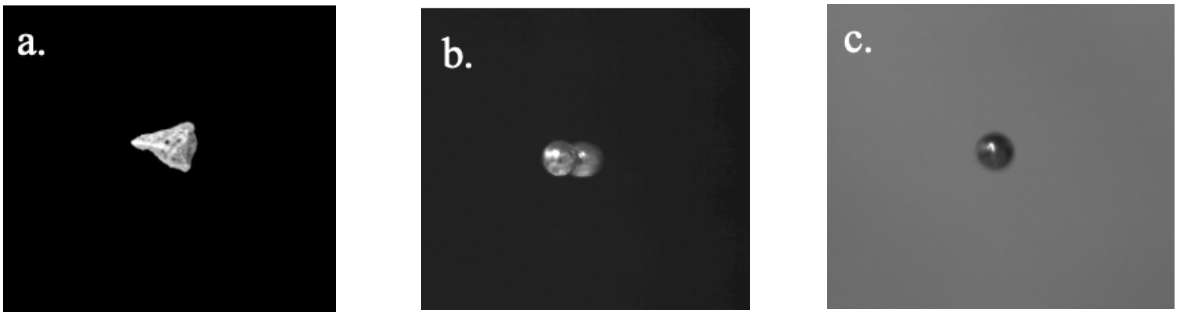

Figure 2.3: New levitation capabilities. Nonuniformly shaped objects (a) may be suspended unlike before. Moreover, we can suspend multiple materials in one node (b). Levitating dense materials like copper (c) is now achievable.

On the upper end of our capabilities, the copper bead (frame c in Figure 2.3) has a density of 8.96 g/cm^3 and a diameter of 2 mm. Relative to expanded polystyrene beads levitated in previous experiments, the copper bead yields an increase in density by a factor of 180 and a simultaneous increase in volume by a factor of 8. Moreover, we have levitated large Styrofoam spheres with a diameter of 4.5 mm. In this case, we are levitating solids with volumes 91 times larger than the small polystyrene spheres from the original levitator.

As shown in frame a of Figure 2.3, we can achieve stable levitation of nonuniformly shaped objects. Typical objects in natural triboelectrically charged granular systems have nonuniformities in their volume and charge distribution. We are excited to implement the new high-powered levitator. We will levitate glass beads coated with films of differing hydrophobicities and discover how hydrophobicity and the rate of charge loss are related.

2.1.2 Charge Measurements

Previous charge measurement techniques in our lab required altering the relative phase of the two hemispheres of transducers. We would place the particle inside the standing wave and fire an ionizer. A 10 kV ion generator would charge the levitated particle with positive or negative electrostatic charge. After waiting a minute or so for the system to equilibrate, we would begin reading the particle's residual charge. By changing the relative phase between the two hemispheres of transducers, the patterns of constructive and destructive interference in the standing wave also changed. We could lower or raise the locations of the nodes, thus changing the location of the trapped particle. The particle would be lowered into a Faraday cage, and the residual charge on the particle would induce a current in the Faraday cage and accumulate a potential difference across a capacitor. Knowing the resistance and capacitance of the Faraday cage system, we could extract a voltage from the particle without ever coming into contact with it. When trying to repeat this charge measurement technique for larger, heavier particles in the new acoustic levitator, the particles consistently would fall out of the wave field. Therefore, we needed an entirely new charge measurement system that would allow us to accurately measure residual charge without ever coming into physical contact with the levitated bead. By vicariously measuring charge, we could ensure that charge was not lost through an external interaction.

Our first hypothesized charge reading system was to move the Faraday cup itself rather than moving the particle. However, we noticed that moving the Faraday cup registered a voltage before the cup had exposure to the particle. We realized that ambient charge was left over on the transducers from the original ionization period. When the Faraday cup moved through this electric field, a current was induced and we registered a voltage. We needed a new charge measurement

technique that would not register ambient charge while accurately reading the residual charge of the levitated particle.

Our proposed charge measurement system utilizes a piezoelectric bender. A piezoelectric bender is a diving-board-shaped device (shown in Figure 2.4) that has two piezoceramic layers sandwiched on top of each other. When an increasing voltage bias is supplied to a piezoceramic material, the length of the material increases. Therefore, by supplying a voltage bias independently in each piezoceramic layer, we can change the relative length of the top and bottom piezoceramic layer. Changing the relative length of one piezoceramic layer gives deflections in the z direction as shown in Figure 2.4.

Figure 2.4: Deflections of the piezoelectric bender. The image was sourced from Thorlabs (the company that produces these piezoelectric benders). When a voltage bias is applied to one piezoceramic layer independent of the other, the bender will deflect in the $\hat{z}$ direction. The bender's resonant frequency is achieved at 370 Hz.

Our proposed theory for how to use a piezoelectric bender as a vicarious charge measurement tool is outlined in Figure 2.5. At the end of the piezoelectric bender, a grounded brass shield extends downward. The grounded shield blocks the electric field lines of the levitated charged particle from a charge sensing copper wire. When a voltage bias is applied to the piezoceramic material, the bender deflects upwards in the $\hat{z}$ direction and the grounded shield rises, exposing the charge sensing wire to the electric field lines of the particle. With exposure to these electric field lines, a current is induced in the wire from which we can extract a voltage on the particle.

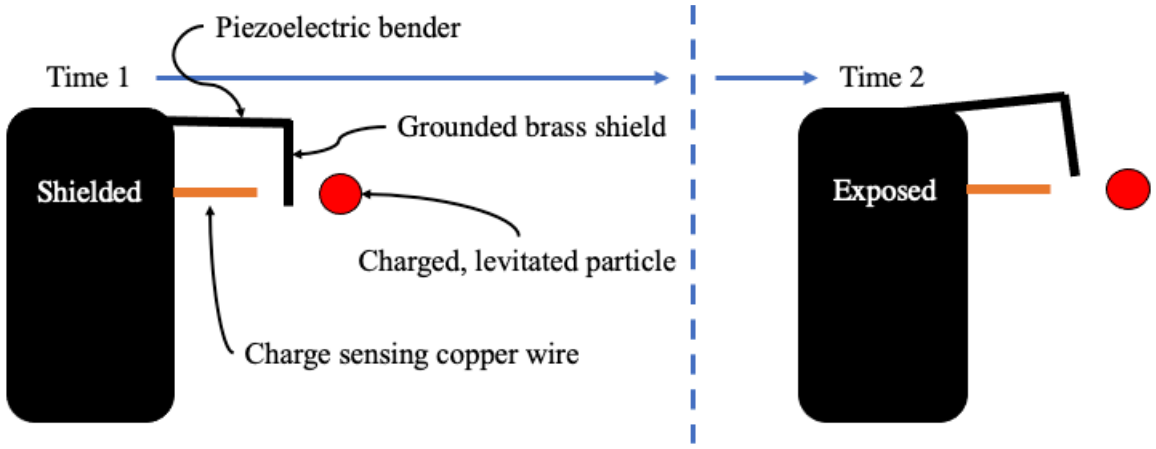

Figure 2.5: The piezoelectric bender charge reading system. At time 1, the piezoelectric bender is in the down position and the grounded brass shield blocks the electric field lines of the levitated particle from the charge sensing copper wire. At time 2, the bender deflects upwards and the wire is exposed to the field lines.

An unloaded piezoelectric bender oscillates at resonance with a frequency of 370 Hz and a maximum displacement of $\pm 450\ \mu$m. However, the weight of the brass shield changes these values. The optimized frequency of operation with the shield attached to the bender is anywhere between 5 and 35 Hz. By moving the shield up and down, the charge that we measure from the particle is insensitive to long term background electrostatic drift – which gives us an accurate charge reading. Within this region of frequencies, at least a particle diameter of deflection is achieved, ensuring that the charge sensing wire has full exposure to the field lines from the levitated particle. Each time the piezoelectric bender is deflected upwards (Time 2 in Figure 2.5), we record a voltage reading. Through the previous Faraday cup measurement technique, we were limited to one measurement every minute. Now, with the piezoelectric bender charge reading system, we achieve multiple measurements per second, giving us an advanced level of precision previously unknown.

2.2 Preliminary Charge Decay Results

2.2.1 Humidity and Discharge Behavior

Over the past year, Burton Lab has collected charge life data for small polystyrene levitated beads in environments of varying humidity. The polystyrene beads were placed into the original acoustic levitator's standing wave field, given a negative electrostatic charge from the ionizer, and moved through a Faraday cup every minute to calculate the voltage on the surface of the bead. These measurements were acquired before the new high powered levitator of the previous section was implemented. Figure 2.6 shows the relationship between relative humidity and the lifetime of charge on a bead.

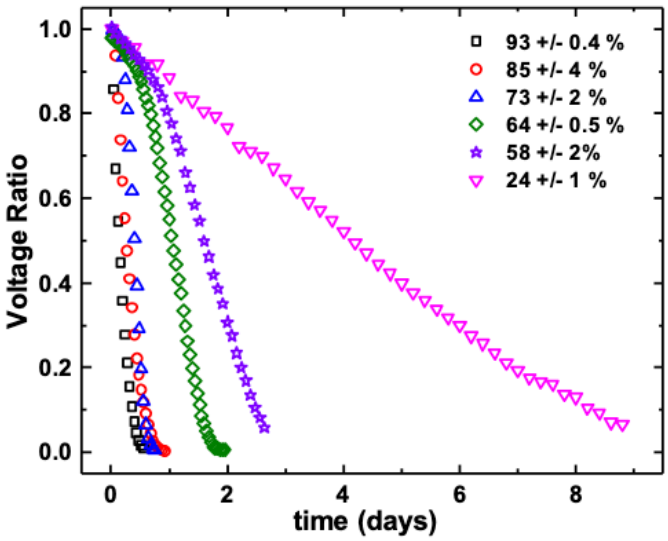

Figure 2.6: Preliminary charge decay results. The relative humidity of each trial is increasing leftward. Charge is lost much faster in wet environments. Levitated particles in dry environments can retain their charge for over a week.

The voltage ratio on the y-axis is defined as the ratio of the particle's voltage at an arbitrary time, t, and the initial voltage from the first charge measurement. Normalizing the particle's voltage allows us to compare different trial runs. From Figure 2.6, charge life is strongly correlated to the relative humidity surrounding the particle. The dominate charge transfer mechanism in humid

environments is effective. The transfer mechanism found in the humid environments could either be ineffective or entirely not present in dry environments – explaining the different charge decay rates observed in high and low humidities.

Following the Langmuir Adsorption model [20], we assume that there are a fixed number of absorption sites on the surface of the polystyrene bead each of which can be occupied by only one charge. Therefore, a charge is either bound to an absorption site by some fixed energy ε or it is in free gas phase without a bound energy. When the levitated polystyrene bead is charged by the ionization gun, copious bound states of energy ε form on the surface of the material. For the charge to be lost from the levitated bead, an external mechanism needs to free the charge from its potential well or an external ion of opposite polarity needs to neutralize the trapped charge. Otherwise, the charge will remain bound to the bead in its potential well.

The photoelectric effect is one hypothesized discharging mechanism. If an incoming UV-photon interacts with one of the bound states, the trapped electron will discharge given that the photon has a sufficient energy to free the charge from its potential well. More data is needed to quantify the dependence of charge decay on the photoelectric effect. Other possible sources of charge transfer could be explained by natural high energy cosmic radiation. High frequency electromagnetic radiation can free electrons from their host molecule and are known to ionize gas. If an incoming gamma ray were to ionize the gas surrounding our levitated particle, then gaseous ions could locate bound states and neutralize them. To test the relationship between high frequency radiation and charge decay, we would need to either surround our experiment with lead bricks or submerge the experiment deep underground. Further work is needed to study the effect that UV

light and high frequency electromagnetic radiation has on charge decay timescales. Because we did not alter these two mechanisms as experimental parameters in Figure 2.6, we assume that these charge decay factors are constant across the trials for now.

Another hypothesized charge transfer mechanism is random air molecule interactions and collisions. As the charged bead floats in the standing wave surrounded by regions of high pressure, random air molecule collisions could bombard the bead's surface and ballistically free bound state charge. Surface vibrations and temperature are another possible charge neutralization mechanism. Assuming that the surface of the levitated particle acts as an Einstein solid, we can conclude the following. On the surface of an Einstein solid, the atoms vibrate as harmonic oscillators where the bonds of the atoms serve as the spring in the analogy to the classical "mass-loaded spring" example from introductory physics. The square of their amplitude of vibration is proportional to the temperature of the system. Typically, atoms at room temperature in thermal equilibrium have vibrational amplitudes of $A \approx 10^{-2}$ nm and oscillation frequencies of $\nu \approx 5 \cdot 10^{12}$ Hz for solid materials. If the vibration energy of the oscillators on the surface of the Einstein solid is sufficiently large, then the bound state can be freed. In both air molecule collisions and surface vibrations, the probability that the interaction will provide sufficient energy to free a bound state follows a Boltzmann distribution. Say that, for example, some energy state ε provides enough energy to free the charge from its potential well. Then, the probability of either the oscillator or air molecule being at this threshold energy is given by the Boltzmann factor $e^{-\varepsilon/kT}$. Therefore, the number of freed bound states per second, r, would be given by the product of this Boltzmann factor and the number of interactions per second.

$$r = e^{-\varepsilon/kT} \cdot \nu, \tag{2.10}$$

where ν is the number of interactions with the bound state charge per second, and the Boltzmann factor describes the likelihood that this interaction is sufficiently large to free the bound state charge.

In the case of the Einstein solid, the number of interactions per second is some percentage of the oscillation frequency (given by $5 \cdot 10^{12}\ Hz$). It must be some percentage of this oscillation frequency because not every oscillation is directly interacting with a bound state charge. In the air molecule collision case, the rate of interaction is the frequency of collisions with the potential well. Collisions from air molecules with the potential well site, however, are much less common. Air molecules are moving around in three dimensional space with random velocities in random directions. The likelihood of a collision within some small surface area dA is not likely. In either case, the rate of freed bound states per second is relatively low as the probability of having a high enough energy ε for a system in thermodynamic equilibrium at room temperature is unlikely.

The photoelectric effect, gamma ray radiation, random air molecule collisions, and surface vibrations are independent of the environment's relative humidity. Thus, these discharge mechanisms do not account for the relationship between the observed neutralization timescales and humidity. Our current theory of what discharging mechanism is critically dependent on humidity stems from water dissociation. Water dissociation is a natural process where a standard H_2O water molecule breaks apart into a positive H^+ hydron ion and a negative OH^- hydroxide ion. In these humid environments, water vapor will condense on the particle's surface and some amount of water dissociation will naturally occur. With positive and negative ions moving around on the surface of the charged particle, these mobilized ions will locate bound state charge and neutralize

it. Gu et al. studied how the byproducts of water dissociation may affect the charging of granular systems [21], however, here we investigate the role of hydron and hydroxide molecules in charge neutralization.

For this following example, we assume that the levitated bead was initially given negative charge by the ionizer. In a humid environment, water condenses on the surface of the bead and water dissociation occurs. Then, the negative OH^- hydroxide ion will leave the surface as it is repelled by electrostatic forces. The positive H^+ hydron ion will locate a negative bound state, neutralize it, then also leave the surface. The hydron and hydroxide ions would play reversed rolls if the particle were given positive charge initially. Given that the only experimental parameter changed in Figure 2.6 was humidity, water dissociation appears to be the dominate charge neutralization mechanism over the other charge transfer devices covered in this section. For a deeper understanding of water dissociation's role in charge loss, we observed charge decay times for beads with both positive and negative charge.

2.2.1 Positive and Negative Charge Decay

Assuming that water dissociation is the key factor in charge loss for the levitated beads, we tested how the rate of charge loss differs for positively and negatively charged polystyrene beads in wet and dry environments. Figure 2.7 displays these results.

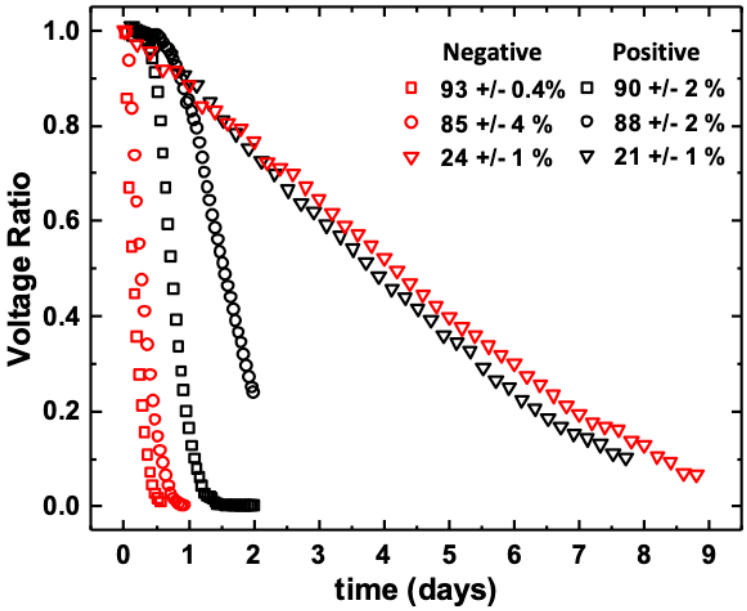

Figure 2.7: The rate of positive and negative charge decay. At high humidities, negative charge (red) is lost much faster than positive charge (black) from the polystyrene beads. The rate of charge loss is independent of charge polarity in low humidities.

The square data points in Figure 2.7 correspond to a relative humidity of 90-93%, and the circle data points were collected from a relative humidity of 85-88%. In both of these cases of very humid environments, the red curve (negative charge) lost all of its residual charge before the black curve (positive charge). The ions resulting from water dissociation are responsible for the observed differences in the rate of charge loss for negative and positive charge. The H^+ hydron ion has a high surface mobility relative to the negative OH^- hydroxide ion. Therefore, we would expect that a particle with negative bound state charges would be neutralized quicker due to the hydron ion's high surface mobility. On the other hand, for a particle given positive bound state charges, the hydroxide ion does not have a high surface mobility and would be less effective in charge neutralization explaining why charge lives longer on positively charged beads.

In dry environments, however, the rate of charge decay appears to be independent of the initial charge polarity of the particle. Therefore, the photoelectric effect, gamma ray radiation, random air molecule collisions, surface vibrations, or other charge transfer devices that are independent of humidity may be the primary force in charge neutralization in this regime. It may also be a combination of these charge neutralizers. Water dissociation must not play a critical role in dry environments because the rate of water condensation on the surface of the particle is not high. Without many water molecules on its surface, a small amount of hydron and hydroxide ions form. And with little charge-neutralizing ions available, positive and negative electrostatic charge is retained for up to a week.

Creating a chart examining the relationship between humidity and charge life, we arrive at Figure 2.8 which shows the half-life of electrostatic charge as a function of relative humidity. The half-life term is a variable that we defined to be the time that it takes for half of the initial electrostatic charge to be lost.

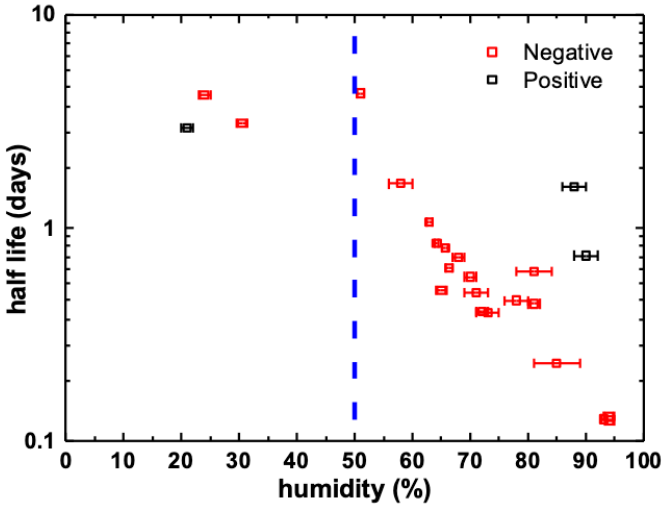

Figure 2.8: Charge half-life as a function of humidity. Half-life is defined as the time for half of the initial charge to be lost. Negatively charged beads decay quicker in humid environments. The rate of charge loss for positive and negative charges is independent of polarity in dry environments.

As seen in Figures 2.6 and 2.7, measuring charge decay can take over week. By defining this half-life variable, we were able to measure twice as much data in the same amount of time. Figures 2.6 - 2.8 indicate that the rate of charge decay is clearly dependent on the humidity of the particle's environment. Also, Figure 2.8 implies that the polarity of the charge matters in humid environments as negative charge is lost much faster than positive charge. Given that the amount of hydron and hydroxide ions formed on the particle's surface dictate the observed timescales of charge decay, we needed to better understand how water films form in environments of varying humidity. Moreover, we want to know how the formation rate of water films depend on a material's hydrophobicity, and how this relates to the observed charge decay timescales of levitated solids. Preliminary measurements with a Quartz Crystal Microbalance were recorded to quantify the rate of water film formation on materials with different hydrophobicities in a hope to create a bridge between charge life and material hydrophobicity.

Chapter 3

Water Film Formations

3.1 QCM Background and Theory

3.1.1 Hydrophobicity and Hydrophilicity

When water lands on a flat, solid surface, one of two things could happen: the water could spread flat, maximizing its contact area on the solid surface or the water could clump-up and form droplets. The angle between the solid and the liquid-gas interface (measured from the inside of the liquid) is defined as the contact angle – denoted by χ. It quantifies the wettability of a surface by a liquid. Figure 3.1 shows the contact angle of water and olive oil on two differently treated aluminum surfaces [22].

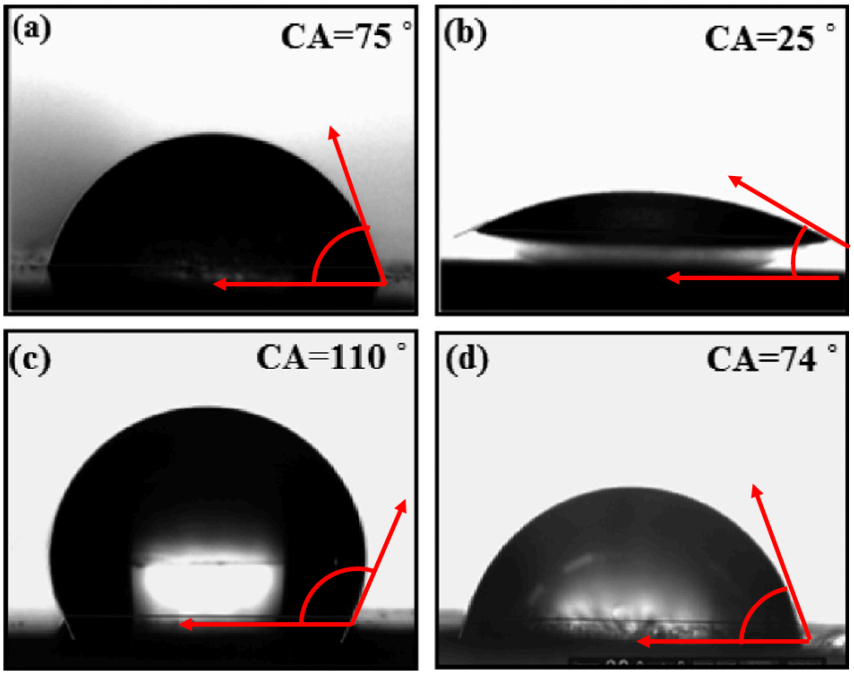

Figure 3.1: Contact angles on differently treated aluminum surfaces [22]. Water is given in frames a and c, and olive oil is given in frames b and d. The interaction on untreated bare aluminum (a and b) is relatively hydrophilic in comparison to modified aluminum (c and d).

Figure 3.1 illustrates the fact that χ is very sensitive to the properties of the fluid and solid involved. The contact angle is a function of both materials combined – it is not an inherent property to either the liquid or solid. The geometry of these liquid droplets allows us to classify their interaction with the solid surface as hydrophilic or hydrophobic. In the case where the water spreads flat and maximizes contact area ($\chi < 90°$), the interaction is said to be hydrophilic and have a high wettability (see frame b in Figure 3.1). However, a material that naturally repels the liquid and causes the formation of droplets ($\chi > 90°$) is said to be hydrophobic (frame c in Figure 3.1). The terms hydrophobic and hydrophilic are derived from Greek roots: hydro, phobia and philos meaning water, fearing, and loving, respectively.

The physics behind contact angles is largely explained by surface tensions [23]. Related to the energy at the surface of a material, surface tension – given by Joules/ m^2 – is defined as the surface energy density and can be thought of as the energy required per unit area to increase the size of the surface. χ of an interacting liquid and solid surface will be hydrophilic for surfaces with relatively high surface energies. The interaction will be hydrophobic for surfaces with relatively low surface energies as the liquid's relatively higher surface tension will hold it in a spherical droplet shape of $\chi > 90°$.

Young's Equation – derived from balancing the surface tensions along the plane of the solid in Figure 3.2 – allows us to calculate χ [23].

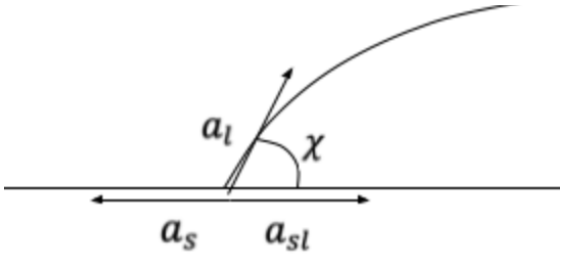

Figure 3.2: Young's equation. Balancing the forces along the plane of the solid leads to the derivation of Young's Equation (3.1). The surface tension, a_s, pulling left must be equal in magnitude to the droplet's, a_l, and solid-liquid's, a_{sl}, tensions pulling right.

$$a_s = a_{sl} + a_l \cdot \cos\chi, \tag{3.1}$$

where a_s is the solid's surface tension, a_l is the liquid's tension, and a_{sl} is the interfacial tension between the liquid and solid. Rearranging Young's Equation, we arrive at Equation 3.2

$$\cos\chi = \frac{a_s - a_{sl}}{a_l}. \tag{3.2}$$

Evaluating the expression above, if the difference of a_s and a_{sl} is large relative to a_l, the right hand side of the equation will be close to 1 and χ must be small. In other words, for relatively large solid surface energies, the interaction will be hydrophilic. On the other hand, if a_l is the dominate term, the right hand side will be close to zero and χ will be large, implying a hydrophobic interaction. Hydrocarbons, polymers, and other plastics historically have low surface energies [24] – that is why after waxing your car, water tends to bead up. On the other hand, most metals and glasses have characterizable high surface energies and are known to be wettable surfaces – example, rain running off of a glass window.

3.1.2 The Sauerbrey Equation

A Quartz Crystal Microbalance – or QCM, pictured in Figure 3.3 – is an extremely sensitive piezoelectric driver and finds use in measuring the mass and thickness of thin-film

deposits [25]. When an alternating current is applied to the quartz crystal, the crystal will begin to oscillate. Considering temperature constant, the QCM will oscillate at a natural, resonate frequency.

Figure 3.3: A quartz crystal microbalance [25]. The circular shaped crystal vibrates at a resonate frequency. According to the Sauerbrey Equation, as mass accumulates on its surface, the rate of oscillation slows.

The Sauerbrey Equation relates the change in oscillation frequency to the change in mass deposited on the surface of the QCM electrodes as Equation 3.3.

$$\Delta f = -C_f \cdot \Delta m \,, \tag{3.3}$$

where Δf is the observed frequency change in Hz, Δm is the change in mass per unit area measured in g/cm^2, and C_f is the sensitivity factor of the crystal given by 56.6 $Hz\ \mu g^{-1}\ cm^2$.

The beauty of the Sauerbrey Equation resides in the fact that, as the foreign film accumulates and mass increases on the QCM surface, the film's thickness of less than 1 micron is much less than the Quart Crystal Microbalance's thickness of 330 microns. Therefore, the film is treated as an extension of the quartz crystal itself and shear forces during vibration are not considered [25]. Thus, C_f does not consider anything about the thin-film layer and the sensitivity factor is defined as a fundamental property of the crystal. Moreover, from Equation 3.3, the thickness of the deposited film can be easily calculated by dividing by the density of the film:

$$T_f = \frac{\Delta m}{\rho_f}, \tag{3.4}$$

where T_f is the thin film thickness in cm and ρ_f is the film's density measured in g/cm^3 (the density of water is 1 $\frac{g}{cm^3}$). At first examination, this equation does not appear to make sense. How can a change in mass per density give units of length? Recall that we defined Δm as the change in mass per unit area. Therefore, after dividing Δm by a density, T_f has units of length. Equation 3.4 is used later in this section to calculate the thickness of water films on QCM surfaces of different hydrophobicities. We hope to pair these QCM measurements with characteristic timescales of charge decay for levitated particles of differing surface hydrophobicities. We hypothesize that the surface hydrophobicity affects the rate of water film formation and the rate of water dissociation, thus affecting the observed charge life on the particle.

3.2 QCM Experimentation

3.2.1 Experimental Design

In order to supplement the overarching project of how electrostatic charge decays as a function of humidity, we needed to better understand water layer formation in humid environments. Our theory of charge decay is dependent on water dissociation in the humid regime, therefore, with a strong understanding of how water layers form in humid environments, more light would be shed on our theory of charge decay.

Figure 3.4 shows our experimental design that analyzes how water films form on different hydrophilic and hydrophobic surfaces.

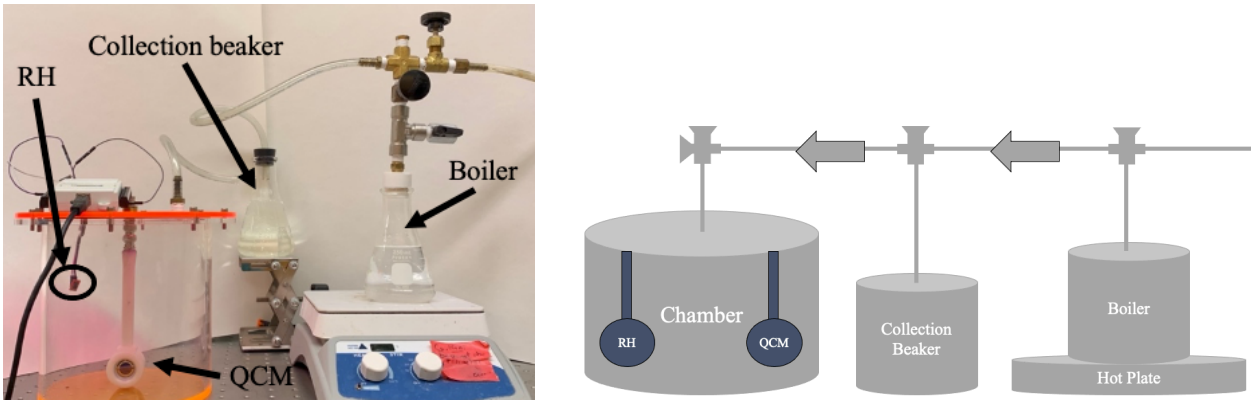

Figure 3.4: Experimental schematic testing water film formation. Cool, dry air flows from right to left, picking up humid air from the boiler along its path. Wet air pollutes the chamber where the RH sensor measures relative humidity and the QCM measures water layer formation.

In Figure 3.4, a constant stream of cool, dry air is pumped from right to left such that a pressure gradient forces the humid air from the boiler to the chamber. As the hot plate heats deionized water, the steam is caught in the draft of the pressure gradient. Flowing down the tube, it reaches another beaker where the stream can condense. In the collection beaker, the hot steam condenses so that macroscopic droplets will not leak onto the surface of the QCM and ruin the trial run. After the steam leaves the collection beaker, it heads for the chamber. The humidity of the chamber rises, measured by the RH (relative humidity) sensor, and the QCM's oscillation frequency slows according to the Sauerbrey Equation. We expect that coating the QCM with different hydrophilic and hydrophobic materials will alter the amount of mass deposited on the surface of the QCM. Chips with low wettability and hydrophobic coatings should not experience large frequency shifts relative to hydrophilic QCM chips. We tested a Gold QCM chip, a glass QCM chip, and a polystyrene coated QCM chip whose contact angles were 45°, 30°, and 90°, respectively.

After collecting data from a few trial runs, we noticed that the rate at which the humidity increased was critical. If, for example, the humidity changed from 20% relative humidity to 90%

within a few minutes, the entire chamber would be saturated with water. To avoid this oversaturation phenomenon, the humidity needed to be increased linearly over a period of a few hours. To accomplish a slow and controlled linear increase of humidity, the temperature of the hot plate was increased in 10 degree increments about every 10 minutes. Trial runs usually lasted one to two hours.

3.2.2 Preparation Prior to Experimentation

Given that the Sauerbrey Equation is only dependent on the external mass on the surface of the QCM, keeping the chip clean before experimentation is imperative. If the chip's surface were contaminated with oils from the skin, dust mites, or any other external mass, it would be reflected in the Sauerbrey Equation, and we would over calculate the deposited water films on the chip's surface.

In order to minimize unwanted excess mass on the QCM surface, a strict cleaning regiment was implemented. The chips were stored in an oven of 50° Celsius when not in use. Before conducting an experiment, the chip was brought to room temperature, submerged in a beaker of ethanol and placed in an ultrasonic bath for 15 minutes. High frequency pressure waves traveled through the ethanol bath and created cavitation bubbles, cleaning the surface of the QCM chip. The chip was then dried by blowing excess ethanol off with pressurized nitrogen gas. The chip was then placed within the QCM holder and data collection began. After the trial, the process of cleaning was repeated and the chip was stored in the oven for future use.

3.3 Results and Discussion

3.3.1 Water Film Thickness Measurements

The first water film thickness measurements taken were with a gold plated QCM. The wettability of gold is described as relatively hydrophilic, where $\chi = 60°$ on average. In our laboratory, we found the contact angle of the gold plated QCM used in experimentation by Figure 3.5.

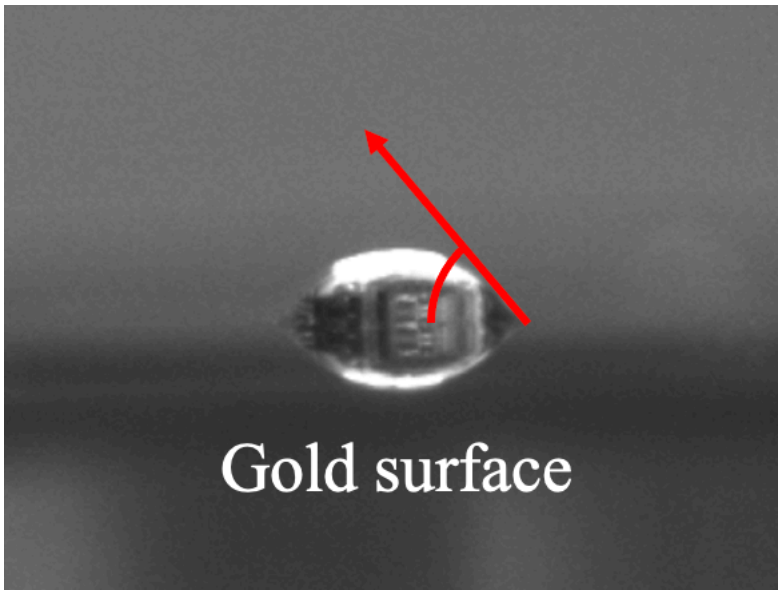

Figure 3.5: Contact angle on a gold surface. Gold has a high surface energy: the interaction of a gold surface and a water droplet is hydrophilic where $\chi \approx 45°$. Film thickness for gold surfaces were measured using a gold coated QCM.

After completing the experimental process described in Section 3.2 for 9 trials, we were able to find the average water film thickness on a gold coating through evaluation of the Sauerbrey Equation. Figure 3.6 shows the formation of water films on a gold surface.

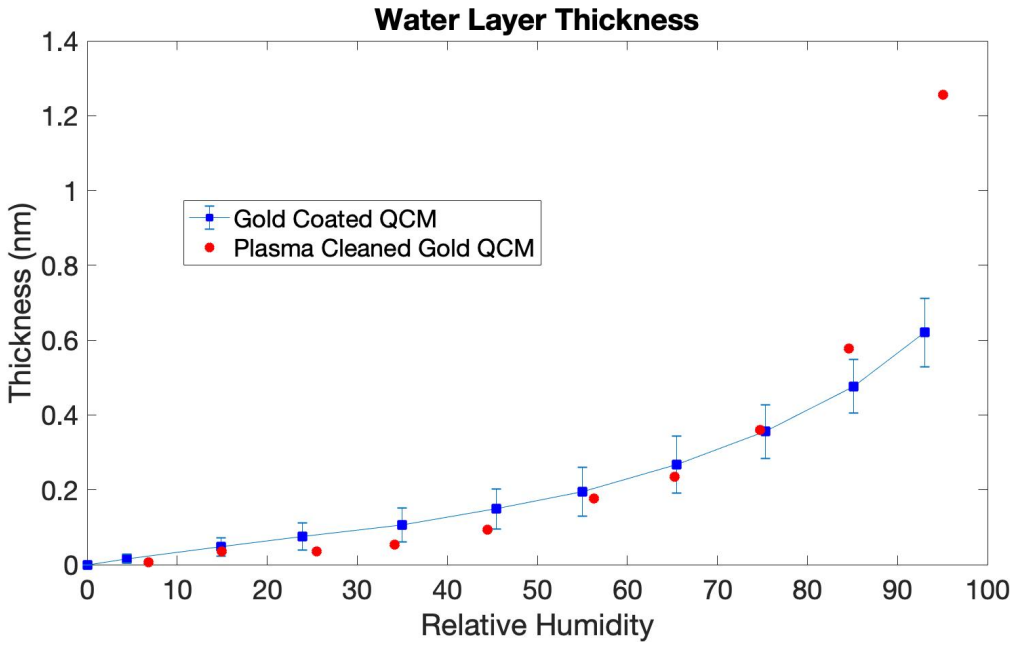

Figure 3.6: Water film formation on a gold surface. As the relative humidity increases, the thickness of the film grows. 2 or 3 monolayers of water form on average. The red data indicates a plasma cleaned gold QCM trial.

In Figure 3.6, the thickness of the water film from each of the nine trials was averaged in ten "bins" of incremental 10 percent relative humidity. The blue bullet points define the average thickness in each bin of humidity. The error bars correspond to one standard deviation from the average. It is known that the thickness of a monolayer of water molecules is 0.25 ± 0.05 nm [27]. Therefore, on average, a total of 2 or 3 monolayers of water accumulated on the surface of the gold QCM. When a film thickness of less than 0.25 nm is calculated in Figure 3.6, we are calculating partial film coverage on the surface. A complete monolayer of water is not formed until the y-axis reads 0.25 nm at about 45% relative humidity.

The hydrophobicity of gold is dependent on the purity and cleanliness of the sample. The purer and cleaner the gold, the more hydrophilic the surface is. We used the process of plasma cleaning to test if our gold sample would be more hydrophilic without surface organic

contaminates. In plasma cleaning, reactive chemicals like oxygen are ionized through high frequency voltages in low pressure environments. The plasma system can break apart organic compounds and clean our sample of any oils or organic materials. The red data in Figure 3.6 corresponds to the thickness of the water film formed on the plasma cleaned gold QCM. One data set was collected for a plasma cleaned gold QCM. Until around 70% relative humidity, the rate of water film accumulation rested within one standard deviation of the mean. However, in humidities greater than 80%, the plasma cleaned gold QCM became saturated with water. At the end of experimentation, 5 layers of water formed; doubling the amount formed on the normal gold QCM sample.

We also conducted experiments with polystyrene coated and glass coated QCM chips. Polystyrene is known to be hydrophobic with $\chi = 90°$, while glass has $\chi = 10°$. Figure 3.7 shows the contact angles observed in our laboratory for the QCM samples used in experimentation.

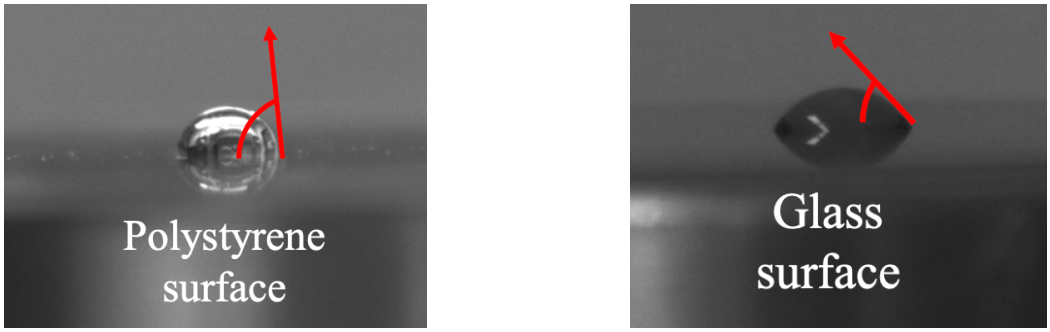

Figure 3.7: Observed contact angles on polystyrene and glass surfaces. Polystyrene (pictured on the left) is hydrophobic, observed $\chi \approx 90°$. Glass (pictured on the right) is known to be hydrophilic, observed $\chi \approx 30°$.

We conducted four trials measuring the film thickness for the glass plated and polystyrene coated QCM. Undergoing the same cleaning process as the gold plated QCM for consistency, we calculated the thickness of the water film in Figure 3.8. As in Figure 3.6, the data points in the

lower plot are averaged into bins of 10 % relative humidity. The error bars indicate one standard deviation from the mean value.

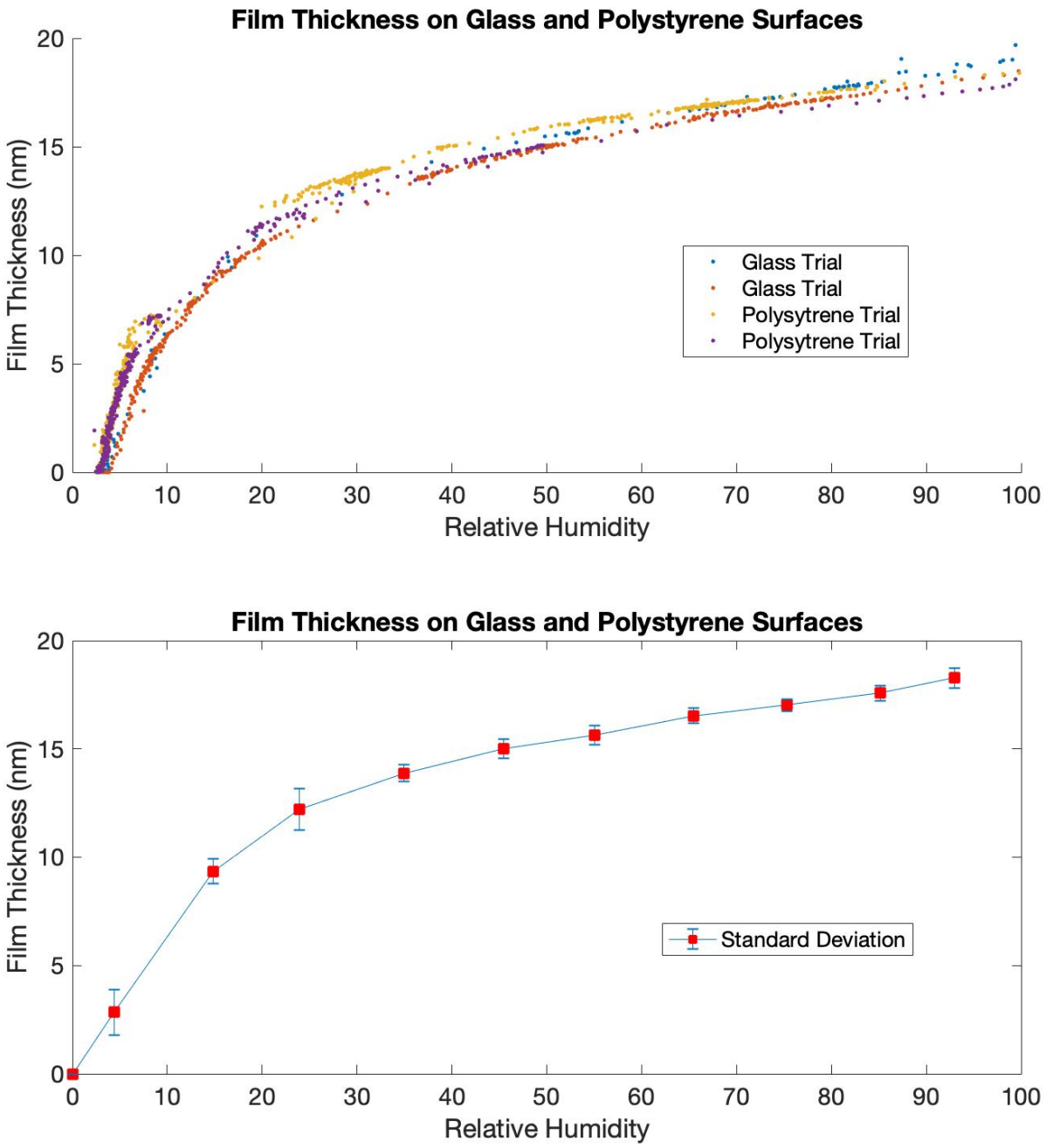

Figure 3.8: Water film formation on polystyrene and glass surfaces. As the relative humidity increases, the thickness of the film grows. Although polystyrene and glass have different hydrophobicities, their accumulation of water films is similar. Both surfaces ended with around 70-75 layers of water.

3.3.2 Interpretation of the QCM Results

The hydrophilic gold, $\chi \approx 45°$, QCM data in Figure 3.6 was cross referenced with data collected by Lazarowich et al. [27]. In a similar process, Lazarowich et al. immersed a gold plated QCM in an environment of increasing relative humidity. At room temperature, water condensed on the surface of the QCM as the humidity increased, causing the rate of the QCM's oscillation to slow according to the Sauerbrey Equation. Figure 3.9 was produced by Lazarowich et al.

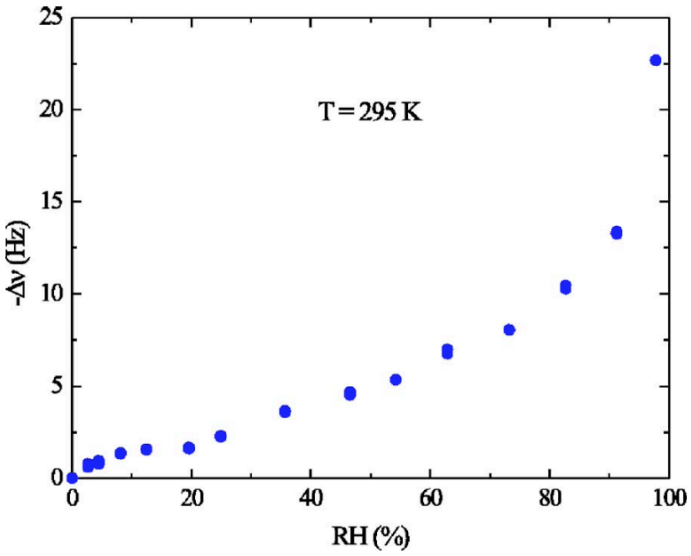

Figure 3.9: Gold QCM damping due to water films by Lazarowich et al [27]. Relative humidity is increased from 0% to 100%, and the rate of the QCM's oscillation slows according to the Sauerbrey Equation.

Water was absorbed onto two sides of the QCM's surface in Figure 3.9. Our experiment, however, only absorbed water from one side of the QCM. Therefore, the data from Lazarowich et al. should be twice as large as ours. Converting $\Delta\nu$ to film thickness on one side of the QCM using Equations 3.3 and 3.4, we find Figure 3.9 corresponds to a maximum film thickness of roughly 2 nm. At 90% relative humidity and dryer, we find a film thicknesses that corresponds with the data collected by our lab in Figure 3.6.

In examining Figures 3.6 and 3.8, there is a clear difference in the rate of water film formation for gold and polystyrene coated surfaces. In Figure 3.6, the gold QCM does not accumulate a film at low humidities: most of the water film is formed in higher humidities. In Figure 3.8, the majority of the film thickness on the polystyrene and glass QCM samples, however, formed in the low humidity region. The concavities of the two curves are opposite, indicating that the microphysical processes responsible for wetting a material are dependent on the materials themselves. Moreover, the magnitude of the film's thickness between the gold and polystyrene surfaces is largely different. The polystyrene coated QCM became completely saturated with 70-75 layers of water whereas the gold plated QCM formed only 2-5 layers. Figures 3.5 and 3.7 indicate that gold is relatively hydrophilic while the polystyrene sample is hydrophobic. Therefore, we would expect the gold to have a higher wettability, yet the opposite is observed.

Porous materials absorb water better than nonporous, solid surfaces. As the surface roughness of a material increases, the material's wettability increases and the interaction is classified as hydrophilic. Gu et al. showed that a copper sample, $\chi = 52°$, can be converted to have super-hydrophilic properties after electrochemical deposition increased the materials surface roughness [28]. Porous materials, like a sponge, have cavities throughout their surface that allow for water and air to absorb into the material. Moreover, materials with rough surfaces expose a larger area of potential water deposit locations and can hold more water than flat, solid surfaces. Figure 3.10 gives a cartoon understanding of water film formation on porous materials.

Figure 3.10: Water film formation on a porous surface. The porous material has cavities and channels where water and air can invade. A porous surface has a higher wettability than nonporous surfaces.

If the polystyrene QCM used in experimentation were porous like in Figure 3.10, then more water than expected would have been deposited on the surface. Even though polystyrene is hydrophobic, a polymer can still exhibit hydrophilic or even super-hydrophilic behaviors by altering the surface roughness of the sample. Lavieja et al. altered the surface roughness of the polymer acrylonitrile butadiene styrene, $\chi = 97°$, with a nanosecond green laser and effectively gave the sample super-hydrophilic properties [29]. We must consider the fact that the polystyrene QCM chip used in experimentation may have been a porous material, giving us a hydrophilic interaction and thicker than expected water films. If we want our polystyrene sample to act hydrophobic, we could treat the sample with the annealing process. Annealing is a process where the porous sample is heated, allowing internal stresses to relax. The weight of the film will flatten itself out, reducing the surface roughness of the material and filling in any cavities on the surface. In future experiments we will anneal the polystyrene film to verify our surface roughness hypothesis.

Although the data did not produce what we expected, this data is still very useful. Expanded polystyrene foam is currently the entirety of our database for charge decay times of levitated solids. So, even though polystyrene itself is hydrophobic, if the expanded polystyrene foam has a high surface roughness, then the material would exhibit high wettability properties

according to Figure 3.8. Therefore, because expanded polystyrene foam has a high surface roughness and thus high wettability, the surface of the levitated particle could have had exposure of up to 75 layers of water on its surface. With copious amounts of water deposited on its surface, there would be many hydron and hydroxide ions traveling around on the surface, which could neutralize bound state residual charge. The data of Figure 3.8 indicates that rough polystyrene is wettable; therefore, the corresponding charge decay times for levitated expanded polystyrene foam should be relatively short as more hydron and hydroxide ions are available.

The polystyrene thin films were coated onto a glass QCM chip. If the glass QCM chip were relatively porous, the polymer film would have relaxed along the contour of the porous glass surface. The similar surface microstructure of the glass and polystyrene films in this case helps to explain Figure 3.8 and why the hydrophilic and hydrophobic films displayed similar wetting properties. On the other hand, the gold surface may have had a low surface roughness. Metals that typically have hydrophilic properties can be altered to display characteristics of hydrophobic surfaces. Qian et al., for example, chemically etched the surface microstructure of a nickel sample to give the normally hydrophobic metal hydrophilic properties [30]. We suspect that the wetting of these thin films is a function of both the material's hydrophobicity and surface roughness.

In all, these QCM measurements help uncover more of the story of how hydrophobicity and surface roughness affect charge decay. To predict the thickness of a water film before it forms, we must know both the surface roughness and hydrophobicity of the material. Relating back to the timescales of charge decay, a film thickness prediction will allow us to estimate the relative amount of charge neutralizing ions (hydron and hydroxide) that are deposited on the surface of a

material. Assuming that water dissociation occurs at a constant rate, thick films will have copious mobile charge neutralizes on their surface, while thin films will not and have longer timescales of residual charge life.

Chapter 4

Conclusions and Future Directions

Burton Lab is currently collecting charge lifetime data for polystyrene levitated beads. The immediate next-step forward for our group is to finish collecting data for polystyrene beads after giving an initial positive or negative charge to the beads (as in Figure 2.7). Our quantitative assessment of charge loss is consistent: charge is lost characteristically faster in humid environments, whereas electrostatic charge can exist in dry environments for over a week. Our qualitative theory explaining the charge transfer mechanisms is a combination of high energy electromagnetic waves freeing charge and thermodynamical disturbances supplying sufficient energy for bound state charges to climb out of potential wells. These mechanisms, however, are insignificant in comparison to our primary theory of charge transfer: water dissociation. In a humid environment, water layers form on the surface of the particle. Water dissociation naturally occurs, forming hydron and hydroxide ions, and the surface of the particle is populated with mobile ions that can neutralize charge. Given that pressure, temperature, and high energy natural electromagnetic radiation were held constant throughout data collection, we assume water dissociation to be the dominate charge transfer mechanism from the data we collected. The timescales that we collected are the first of its kind, and no other research team has used acoustic levitation as a scientific tool for studying charge decay.

For a future paper, our lab wants to answer the question of "at what rate do water films form on different materials, and can a connection between film thickness and charge life be made?" Our lab will take further QCM measurements for a deeper understanding of how hydrophobicity,

surface roughness, and porosity affect water film formation, thus giving an estimation for the number of mobile ions on a particle's surface. With an understanding of the amount of mobile surface ions, we will be able to predict charge life. We will coat an array of QCM chips with materials of varying wettabilities and study the rate of water film formation on these films. With a database of film thickness measurements, we will then implement the new high powered levitator. We will study the rate of charge leakage on glass beads coated with the same films from our database of film thickness measurements. We hope to create a map between film thickness and charge life as follows.

Material	**Film Thickness**	**Charge Life**
Polystyrene	70-75 monolayers (Porous??)	Humid: day or less Dry: week or more
Gold	2-5 monolayers (Low surface roughness??)	???
Glass	70-75 monolayers (Porous??)	???

Figure 4.1: Film thickness to charge life map. Burton Lab will complete this table that measures the film thickness formed on a material and the corresponding lifetime of charge on that material. Glass beads and QCM surfaces will be coated with the same films, and these results will be studied in pairs.

We hope that the marriage of these QCM measurements and our high powered levitator will affirm our hypothesis that water dissociation is the dominate factor in the rate of charge loss. The pairing of an acoustic levitator and a QCM to study the rate of charge leakage and the charge transfer mechanisms involved has not been done before. Future measurements are needed for a deeper

understanding of our hypothesized charge transfer mechanisms; however, these preliminary timescales of charge loss are the first of their kind.

Bibliography

[1] Blum, J., & Wurm, G. (2008, September 22). The growth mechanisms of macroscopic bodies in protoplanetary disks. *Annual Review of Astronomy and Astrophysics.*

[2] Steigerwald, B., & Dunbar, B. (2006, July 31). Electric dust storms on Mars. *NASA Goddard Space Flight Center.*

[3] Navarro-González, R., & Segura, A. (1970, January 01). Volcanic lightning and the availability of REACTIVE nitrogen and phosphorus for CHEMICAL evolution: Semantic Scholar. *Springer, First Steps in the Origin of Life in the Universe, 201-210*

[4] Gray, E., & Garner, R. (2015, February 24). Saharan dust Feeds AMAZON'S PLANTS. *NASA Earth Science News Team*

[5] University of Maryland. (2015, February 24). Massive amounts of Saharan dust fertilize the Amazon rainforest. *ScienceDaily*.

[6] Kahn B. (2015, February 25). How Sahara Dust sustains the Amazon rainforest, in 3-D. *Climate Central.*

[7] Zhang, H., & Zhou, Y. (2020, October 08). Reconstructing the electrical structure of dust storms from locally observed electric field data. *Nature Communications, 11, 5072*

[8] Merceret, F., Ward, J., Mach, D., Bateman, M., & Dye, J. (2008, January 01). On the magnitude of the electric field near THUNDERSTORM-ASSOCIATED CLOUDS. *Journal of Applied Meteorology and Climatology, V47, 240-248*

[9] Perkins, S., (2016, July 8). Static electricity strengthens desert dust storms. *American Association for the Advancement of Science.*

[10] Shinbrot, T., & Herrmann, H. (2008, February 13). Static in motion. *Nature, V451, 773-774*

[11] Tada, Y., & Murata, Y. (1995). Direct charge leakage through humid air. *Japanese Journal of Applied Physics*, 34(4R):1926, 1995.

[12] Marzo, A. (2020). Standing waves for acoustic levitation. *Acoustic Levitation,* 11-26. doi:10.1007/978-981-32-9065-5_2

[13] Fontana, S., Liu, I., Moeller, D., & Robins, K. (2016, July 22). Acoustic Levitation: A Theoretical Exploration. *New Jersey Governor's School of Engineering and Technology*

[14] Nave, R. (n.d.). Standing waves. *Georgia State University, HyperPhysics*

[15] Bruus, H. "Acoustofluidics 7: The acoustic radiation force on small particles." Lab Chip, 12, 1014 (2012).

[16] Gor'kov, L. P. "On the forces acting on a small particle in an acoustical field in an ideal fluid." Soviet Physics Doklady, 6, 773 (1962).

[17] Foresti, D., Nabavi, M., & Poulikakos, D. "On the acoustic levitation stability behavior of spherical and ellipsoidal particles." J. Fluid Mech., 709, 581-592 (2012).

[18] Wortsmann, L. (2016, May 12). Stability of a Particle Levitated in an Acoustic Field.

[19] Marzo, A., Barnes, A., & Drinkwater, B. "TinyLev: A multi-emitter single-axis acoustic levitator." Rev. Sci. Instr., 88, 085105 (2017)

[20] Swenson, H., & Stadie, N. P. (2019). "Langmuir's theory of Adsorption: A Centennial Review." *Langmuir, 35*(16), 5409-5426. doi:10.1021/acs.langmuir.9b00154

[21] Gu, Z., Wei, W., Su, J. et al. "The role of water content in triboelectric charging of wind-blown sand." *Sci Rep* 3, 1337 (2013)

[22] Barthwal, S., Kim, Y. S., & Lim, S. (2013). "Mechanically robust superamphiphobic aluminum surface with nanopore-embedded microtexture." *Langmuir, 29*(38), 11966-11974. doi:10.1021/la402600h

[23] Lautrup, B. (2019). *Physics of continuous matter: Exotic and everyday phenomena in the macroscopic world* (Second ed.). Boca Raton, FL: CRC Press.

[24] Owens, D. K., & Wendt, R. C. (1969). Estimation of the surface free energy of polymers. *Journal of Applied Polymer Science, 13*(8), 1741-1747. doi:10.1002/app.1969.070130815

[25] Stanford Research Systems. (2018, June). QCM200 Quartz Crystal Microbalance Digital Controller.

[26] Opitz, A., Scherge, M., Ahmed, S. I., & Schaefer, J. A. (2007). A comparative investigation of thickness measurements of ultra-thin water films by scanning probe techniques. *Journal of Applied Physics, 101*(6), 064310. doi:10.1063/1.2712155

[27] Lazarowich, R. J., Taborek, P., Yoo, B., & Myung, N. V. (2007). Fabrication of porous alumina on quartz crystal microbalances. *Journal of Applied Physics, 101*(10), 104909. doi:10.1063/1.2730563

[28] Gu, H., Wang, C., Gong, S., Mei, Y., Li, H., & Ma, W. (2016). Investigation on contact angle measurement methods and wettability transition of porous surfaces. *Surface and Coatings Technology, 292*, 72-77. doi:10.1016/j.surfcoat.2016.03.014

[29] Lavieja, C., Oriol, L., & Peña, J. (2018). Creation of Superhydrophobic and Superhydrophilic surfaces on ABS employing a NANOSECOND LASER. *Materials, 11*(12), 2547. doi:10.3390/ma11122547

[30] Qian, X., Tang, T., Wang, H., Chen, C., Luo, J., & Luo, D. (2019). Fabrication of hydrophobic NI surface by chemical etching. *Materials, 12*(21), 3546. doi:10.3390/ma12213546

[31] Gnip, I., Kersulis, V., Vejelis, S., & Vaitkus, S. (2006). Water absorption of expanded polystyrene boards. *Polymer Testing, 25*(5), 635-641. doi:10.1016/j.polymertesting.2006.04.002

[32] Atreya, S., Wong, A., Renno, N., et al. "Oxidant enhancement in Martian dust devils and storms: implications for life and habitability." *Astrobiology*, 6(3):439–450, 2006.